Appl. Phys. 13, 245—253 (1977)

Applied Physics
© by Springer-Verlag 1977

Structure Investigations on Single-Crystal Gold Films

W. Fischer, H. Geiger, P. Rudolf, and *P. Wissmann*

Institut für Physikalische und Theoretische Chemie,
Universität Erlangen-Nürnberg, D-8520 Erlangen, Fed. Rep. Germany

Received 28 December 1976/Accepted 16 February 1977

Abstract. Structure of epitaxially grown gold films of varying thickness (10–1000 Å) has been investigated using LEED, AES, resistivity measurements and X-ray diffraction analysis. Silicon 111-oriented crystals, which are prehandled to exhibit $\sqrt{3} \times \sqrt{3}\, R\, 30°$-superstructure in the LEED pattern, serve as substrates. The gold films show a homogeneous structure with smooth surfaces and a marked (111)-orientation. The use of silicon substrates, however, is complicated by the fact, that silicon diffuses through the gold films to a small extent even at room temperature.

PACS Code: 68.50

Gold films deposited on silicon substrates play an important role in industrial applications like integrated circuits [1] and other semiconductor devices [2]. Besides this they may serve as adsorbent in investigations of the "structural factor" involved in heterogeneous catalysis [3]. Structure properties of such films have, therefore, found wide interest in many papers in the past. Nucleation process has been studied thoroughly [4, 5]. Silicide formation at higher temperatures has also been investigated intensively [6, 7]. On the other hand, the effect of substrate orientation and film thickness on structure has been considered in only a few papers [8].

The interpretation of the electrical [9] and catalytic [3] properties of thin films is simplified if single-crystal films with a well-defined orientation are used. But it comes out, that the structure of such single-crystal films may differ considerably from the structure of the corresponding bulk single-crystals. The aim of the present paper is, therefore, to study this difference for the system Au/Si in the thickness range 10–1000 Å. LEED, AES, resistivity measurements and X-ray diffraction analysis have been utilized for these experiments. Simultaneous application of these four independent methods on the same films allows us to present a relatively accurate picture of the structural properties of the films.

1. Pretreatment of the Silicon Substrates

The slightly boron-doped silicon substrates (Wacker & Co., Burghausen, dimensions $20 \times 10 \times 1$ [mm], $\varrho > 500\,\Omega$cm) were polished chemically with the usual etching method [10]. After setting the silicon substrates in a modified crystal fixture of a LEED/AES apparatus (Varian, type 120), the crystals could be heated up to temperatures of 1450 K by passing direct current through them.

Mainly oxygen and carbon left-overs remain as impurities on the substrate surface, as seen in the Auger spectrum. Traces of nitrogen are also weakly discernable. Figure 1 shows the intensity distribution of Auger peaks of oxygen (516 eV) and carbon (270 eV), referring to Auger signal of the 92 eV silicon transition of the

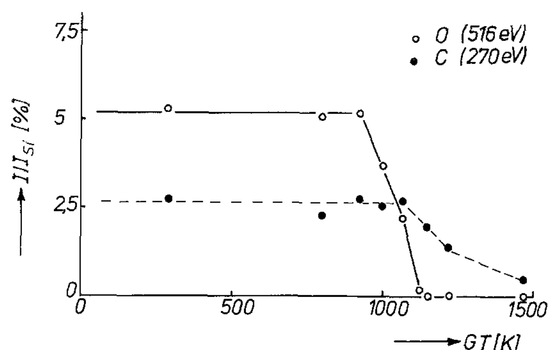

Fig. 1. Dependence of relative Auger peak heights of impurities on the silicon surface on glow temperature

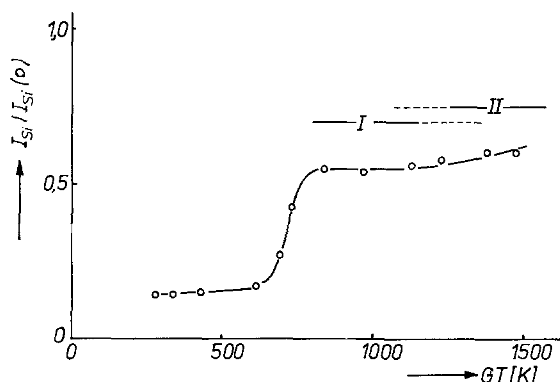

Fig. 2. Increase of the Si (92 eV) Auger peak height during heating up a 20 Å thick gold film. Region I: $\sqrt{3} \times \sqrt{3}\,R\,30°$-superstructure. Region II: 6 × 6-superstructure

clean surface. The peak intensity depends strongly on the temperature *GT*, at which the crystals in the UHV were glowed before evaporation. This temperature was regulated by the current density and measured quite accurately using a calibrated pyrometer.

The Auger intensities remain approximately unchanged up to 900 K, as seen in Fig. 1. At higher temperatures, oxygen peak becomes smaller (simultaneously mass spectrometer shows an increasing CO-peak in the gas phase). At 1100 K silicon surface is almost free of oxygen, although quite large quantity of carbon can still be detected. The carbon impurities of the surfaces can be reduced further, but not completely, if one glows the crystal at still higher temperatures.

Si(111)-crystals show a typical 7 × 7-superstructure LEED pattern [11, 12] after the heat treatment at 1100 K. The $\sqrt{3} \times \sqrt{3}\,R\,30°$-superstructure [6], which favours epitaxial growth of gold films, can be obtained by depositing about 20 Å thick gold films on the glowed crystal and repeating the whole heat treatment process. In this case the Si (92 eV) Auger peak depends on glow temperature *GT*, as shown in Fig. 2. Auger intensities are normalized to $I_{si}(o)$, which was obtained before depositing gold. One recognizes from Fig. 2, that the silicon peak increases rapidly above 600 K with increasing glow temperature. It is interesting to note, that this increase happens just in the temperature region, in which compact Au/Si alloys show eutectic behaviour ($T_e = 640$ K, Si: 69 %, Au: 31 % [13]). Therefore, the assumption, that a quasi-liquidlike behaviour of Au/Si films on the surface of silicon substrates is responsible for the rapid increase of silicon signal, is quite plausible. At about 800 K the silicon signal reaches a marked plateau. Here the $\sqrt{3}$-superstructure becomes evident (Region I in Fig. 2). On further heating, the superstructure changes into 6 × 6

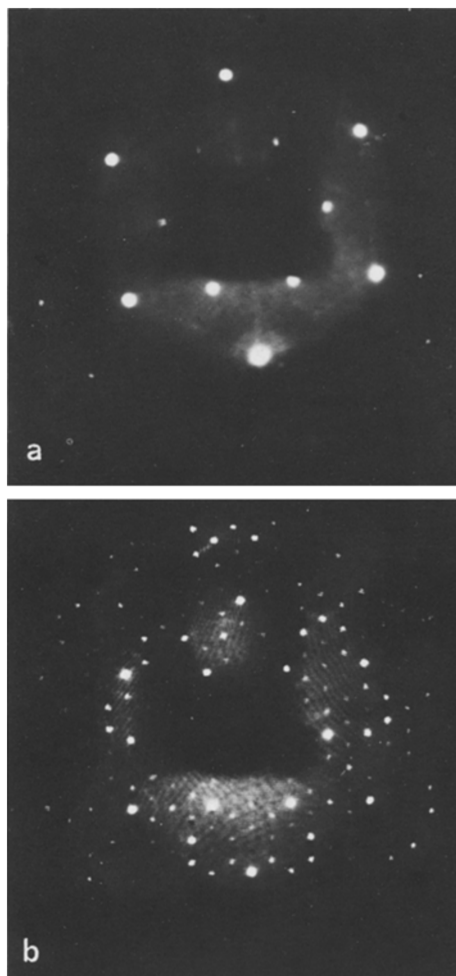

Fig. 3a and b. LEED pattern of a silicon $\sqrt{3} \times \sqrt{3}\,R\,30°$-superstructure (a) and a 6 × 6-superstructure (b)

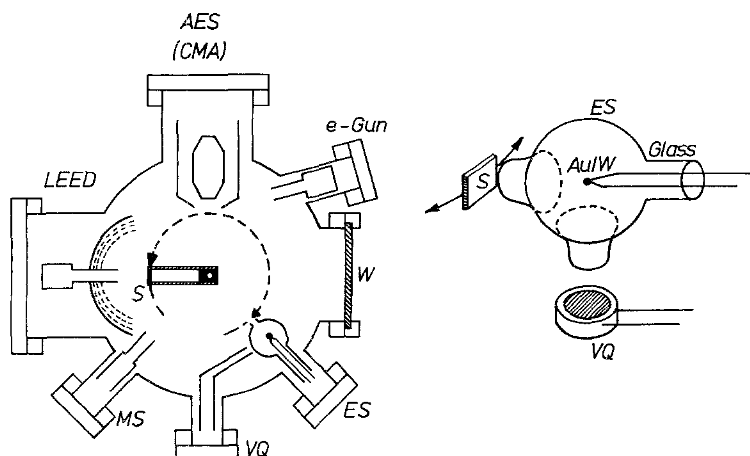

Fig. 4a and b. UHV apparatus (a) and arrangement of the film thickness monitor head (b), schematically. (W: window, ES: evaporation source, VQ: vibrating quartz oszillator, MS: mass spectrometer, S: silicon substrate)

[16, 6] (Region II in Fig. 2, the corresponding LEED patterns are shown in Fig. 3). It becomes obvious from Fig. 2, that the silicon surface contains detectable amount of gold even at the highest glow temperature. Numerous experiments have shown that deposition of gold at room temperature on the $\sqrt{3}$-superstructure results in a relatively well (111)-oriented single-crystal gold film structure. Such films come nearest to bulk single crystal with respect to electrical and catalytic properties and, therefore, are the subject of our interest in the following. All other deposition parameters were kept constant as carefully as possible in order to achieve comparable conditions. If instead of $\sqrt{3}$-superstructure the films are deposited on Si-substrates prepared in some other way, film properties may change considerably [8].

2. LEED and AES Measurements

The vacuum chamber is shown in Fig. 4a schematically. Pressures down to $1 \cdot 10^{-10}$ Torr can be obtained easily. Experimental details are described elsewhere [15]. In Fig. 4b some details of the arrangement of the bakeable thickness monitor head VQ (type Kronos QM 300) and the evaporation source ES are given. The silicon substrate can be manipulated from outside either towards the evaporation source or towards LEED optics/Auger electron analyser.

If gold is deposited at a rate of 10 Å/min at room temperature on the $\sqrt{3}$-superstructure, then at first the LEED pattern disappears and the background brightens up. At about 50 Å the typical Au(111) diffraction pattern appears weakly for the first time, at 100 Å the contrast becomes much better. The sixfold symmetry of the LEED pattern is seen quite clearly from Fig. 5a, although the diffraction maxima are broadened appreciably in azimuthal directions. Besides there are two symmetrically situated satellite peaks detectable for each diffraction maximum. These satellites disappear with increasing thickness, and the azimuthal broadening decreases remarkably. At 700 Å thickness so sharp maxima can be seen (Fig. 5c), that the diffraction pattern can hardly be differentiated from bulk patterns. Evaluation of AES spectra leads to the thickness dependence shown in Fig. 6. The 92 eV Auger peak of silicon decreases at the beginning quite rapidly and arrives than at a saturation plateau. Additionally the figure contains a theoretical curve (dotted curve), which has been calculated according to the relation [16, 17]

$$I_{si}(d)/I_{si}(o) = \exp(-d/\Lambda). \quad (1)$$

Here, d is the film thickness, $I_{si}(d)$ and $I_{si}(o)$ are the intensities of the Si (92 eV) peak after and before film deposition, respectively, and Λ is a free parameter which is chosen to bring the curves to agreement at the initial stages of film formation. This adjustment leads to $\Lambda \cong 4$ Å. The quantity Λ can be correlated to the attenuation length l_0 of the 92 eV electrons, if a correction factor is introduced in order to take into account the geometrical arrangement of the Auger electron analyser. Performing this correction results in $l_0 \cong 5$ Å, which is in good agreement with literature values [16, 18].

For higher thicknesses, however, the measured peak intensities lie clearly above the calculated curve, as seen in Fig. 6. In order to understand this discrepancy it is necessary to analyse the exact form of silicon Auger signals instead of evaluating peak heights only. The form changes with changing thickness as seen in Fig. 6b. The Si (92 eV) peak shows the normal structure with a

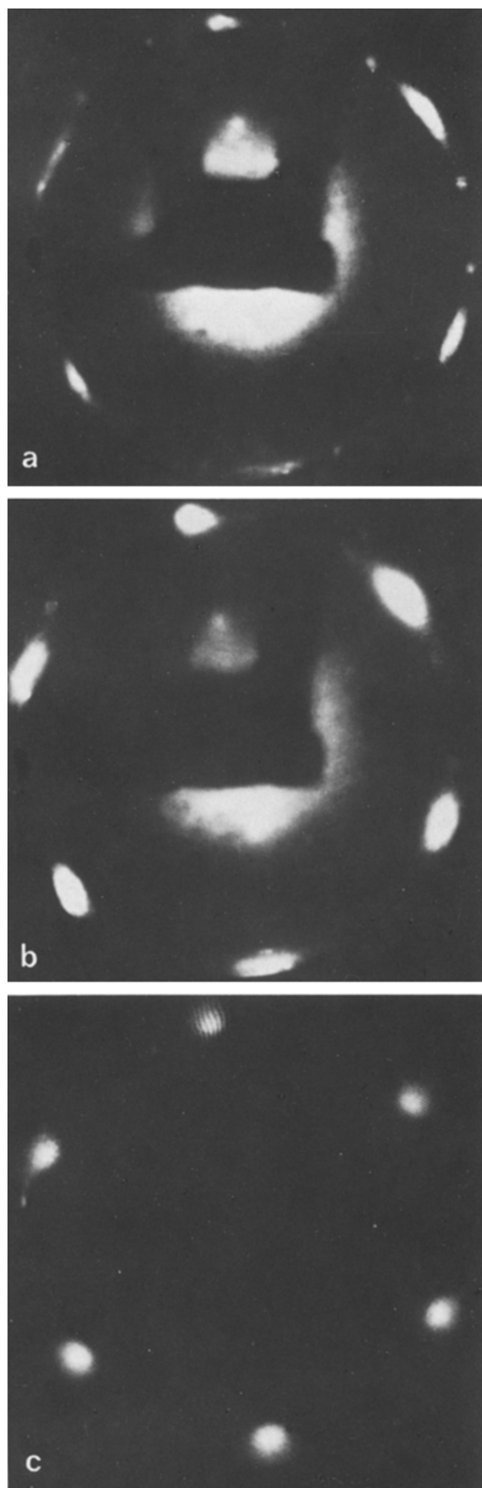

Fig. 5a–c. Dependence of LEED pattern of evaporated gold films on film thickness (a) $d=100$ Å, (b) $d\approx300$ Å, (c) $d=700$ Å. $U\cong40$ V, measuring temperature MT = 293 K

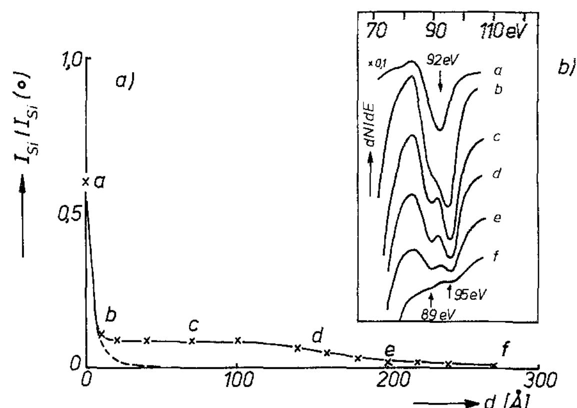

Fig. 6a and b. Height (a) and shape (b) of the Si (92 eV) Auger peak in dependence on thickness of the evaporated gold film

marked minimum in the differentiated spectrum only for the pure $\sqrt{3}$-superstructure. With increasing thickness of the evaporated gold film a shoulder grows in the smaller energy region, and the minimum is displaced towards higher energies. Above 20 Å there are two separated minima distinguishable at 89 and 95 eV, respectively. This result contradicts the opinion, that a coagulation of gold film is responsible for the presence of the silicon Auger peak at higher thicknesses. The splitting rather points to the fact, that silicon diffuses up to the film surface region already at room temperature, and exhibits an electronic state quite different from the bulk. Similar splitting has been observed by Hiraki et al. [19] on Au/Si, and by Grant and Haas [20] on Cu/Si system. Whether the splitting is to be attributed to cross transitions, as has been discussed by Müller et al. [21] in the case of transition metal oxides, or is to be explained by redistributing electron state density in silicon at the film surface, cannot be decided as yet. It is interesting to note, however, that above thicknesses of 300 Å the diffusion of silicon through gold is hindered to such an extent, that silicon can no longer be detected at the film surface at room temperature (see Fig. 6).

3. X-Ray Diffraction Analysis

After finishing LEED and Auger measurements the gold deposited silicon crystals are taken out of the UHV chamber and set in a X-ray texture analyser or in a normal goniometer analyser. Ray path in texture analyser is shown in Fig. 7 schematically. Usual evaluation procedure [22, 23] yields pole figures as shown in Fig. 7 for 200 Å thick (a) and 700 Å thick (b) gold films. The lines plotted in the pole figure represent lines

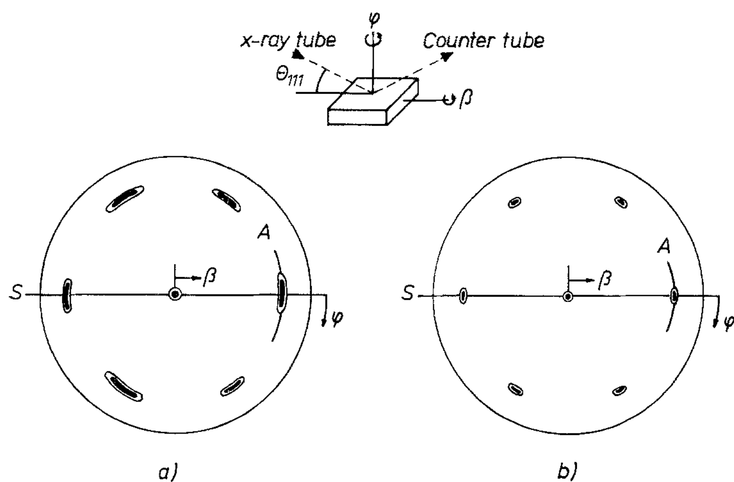

Fig. 7a and b. X-ray beam path in a texture analyer (schematically) and (111) pole figures obtained for a 230 Å thick (a) and 700 Å thick (b) gold film

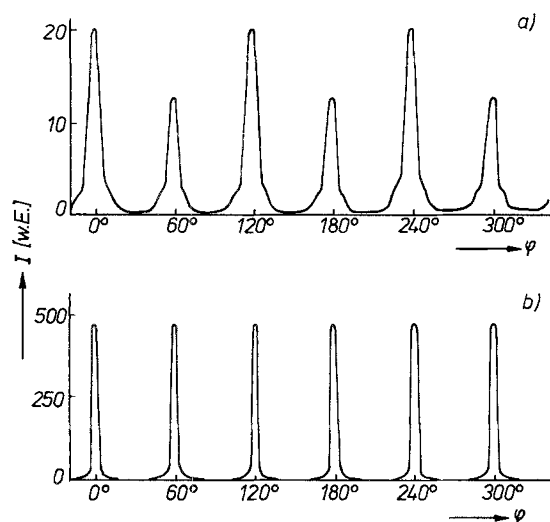

Fig. 8a and b. Azimuthal dependence of the diffracted intensity taken along the crossing lines A in Fig. 7. (a) $d=230$ Å, (b) $d=700$ Å

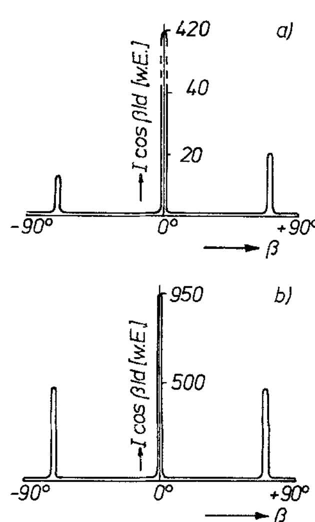

Fig. 9a and b. Radial dependence of the diffracted intensity taken along the crossing lines in Fig. 7. (a) $d=230$ Å, (b) $d=700$ Å

of equal intensity, the meaning of β and φ can be taken from the small insertion at the top of Fig. 7.

Instead of showing the typical threefold symmetry of (111)-planes in fcc metals the pole figure offers a sixfold symmetry. Obviously the films contain twinning faults which may be situated either in the film plane or perpendicular to film plane. The side maxima are observed at the β-value of 70.5°, which is in good agreement with the theoretical prediction for fcc metals [23]. But it should be mentioned, that for the thinner films the six side maxima are not of equal intensity, three of them being higher (Fig. 7a).

Following the intensity along the crossing lines A and S drawn in Fig. 7 leads to the texture profile shown in Figs. 8 and 9. The azimuthal broadening of the side maxima already known from LEED pattern of thin gold films is seen explicitly in Fig. 8a. There are weak shoulders observable in the azimuthal dependence of side maxima, which also correspond well with the LEED pattern of Fig. 5b. On the other hand, sharp satellite peaks cannot be resolved even in the case of thinner films.

The influence of peak broadening due to the limited resolving power of the diffraction set-up can be estimated by measuring the radial and azimuthal width at half-maximum intensity (β_{hr} and β_{ha}) for a compact Au(111) single-crystal serving as standard. These values are put together in Table 1 along with the film values. One can see easily, that the broadening due to the films is in each case larger than the instrumental broadening.

Table 1. Comparison of peak broadening of the films with the instrumental broadening, obtained for a compact Au (111) single-crystal

Material	β_{hr}	β_{ha}
Film (d = 230 Å)	2.0°	11°
Film (d = 700 Å)	1.7°	4°
Bulk single crystal	0.3°	1.0°

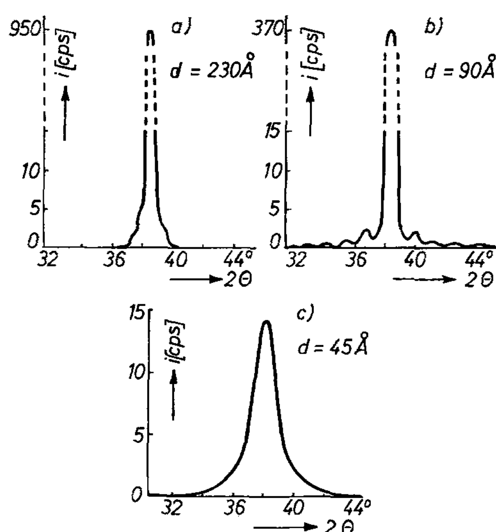

Fig. 10a–c. Dependence of the diffracted intensity on the double Bragg's angle 2θ for (111)-oriented gold films. (a) $d = 230$ Å, (b) $d = 90$ Å, (c) $d = 45$ Å

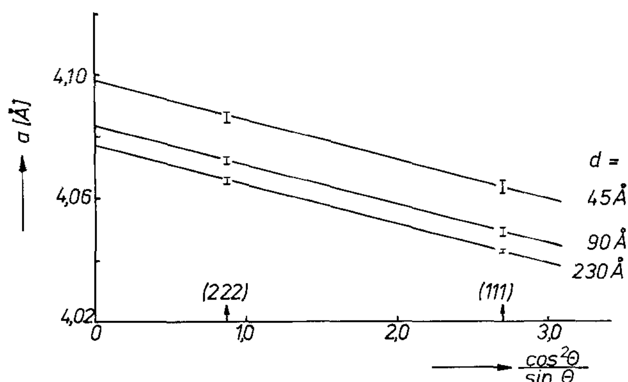

Fig. 11. The quantity a' [refer to (2)] obtained for the (111) and (222) reflex in a plot against $\cos^2\theta/\sin\theta$ in order to eliminate adjustment errors

The gold films, therefore, must process a mosaic structure [24], i.e. the crystallites are inclined against each other to a certain degree.

In goniometer analysis only (111) and (222) peaks can be detected because of the largely (111)-orientation of the films. The broadening of these Bragg peaks increase, as expected, with decreasing thickness strongly [25]. Figure 10 shows this for three typical gold films of different thicknesses. Here, the intensity of diffracted X-rays is plotted against the double Bragg angle 2θ. The peaks show always a symmetric form. It is interesting to note, however, that for the 90 Å thick film numerous satellite maxima are distinctly observable. Such satellite maxima can be correlated to the relatively small number of lattice planes taking part in diffraction [25, 26]. The fact, that the satellite maximum of sixth order can be detected with sufficient accuracy, allows us to conclude, that the film possess an extra-ordinarily plane parallel structure. If the thickness were to fluctuate around some mean value, then the satellites of higher order should disappear due to interference [26]. Quantitative analysis of the curves of Fig. 10 must remain, however, the topic of a future publication [27] due to space reasons.

The (111)-reflex can be measured very accurately even for 45 Å thick films as seen in Fig. 10. The high sensitivity has been achieved by means of doubly focussing crystal monochromator, step scanning unit and impulse height discriminator. Moreover, well-oriented single-crystal films favour a high intensity of the diffracted X-rays. In this way a critical film thickness of about 100 Å, which is usually regarded as the lowest limit for X-ray diffraction analysis of thin films [26], can be further reduced drastically.

From the exact position of the (111) and (222) peaks the quantity a' can be calculated using Bragg's equation [25]

$$a' = \lambda \sqrt{h^2 + k^2 + l^2}/2\sin\theta, \tag{2}$$

where θ is Bragg's angle, (hkl) Miller's indices and λ the wavelength of the Cu-$K\alpha_1$ X-rays. In order to eliminate adjustment errors, it is usual to plot the a'-values against the quotient $\cos^2\theta/\sin\theta$ [25]. The lattice constant a, then, is determined by extrapolating linearly to the value $\cos^2\theta/\sin\theta = 0$. This extrapolation is shown in Fig. 11 for the three films discussed already in Fig. 10. The lattice constants obtained in such a way are plotted in Fig. 12 against film thickness. Additionally the figure contains a dotted line indicating the a-value obtained for the compact Au metal (4.0784 Å [28]). Lattice constants for thick films are seen to come closest to the bulk value. In the case of thinner films, however, a-

values are found to be too high, as has also been reported by Vook et al. [29] for the system gold/glass. These authors proved their results to obey, quantitatively, the relation

$$a = a_0 + A/d, \tag{3}$$

where a_0 and A are two characteristic constants and d is film thickness. The equation has been obtained by assuming, that the uppermost lattice planes are separated from each other by a distance larger than inside the bulk.

In the present paper, no thickness dependence of a-values is observed above 200 Å. For thicknesses below 200 Å an increase in a-values occurs, which is much steeper than would be expected according to (3). Moreover, a-values fluctuate rather strongly indicating the important influence of other preparation parameters than the thickness. Therefore, the application of (3) cannot be justified in the present case.

Apart from the peak position, the broadening and the intensity of the peak can be evaluated. Moreover, the complete peak profile may be analysed by Fourier transformation [25]. All these evaluations have been performed additionally. They do not lead, however, to any important new information. Only previous results [8] are confirmed, namely: a) The mean crystallite size, which refers to the crystal dimensiones perpendicular to the film plane, comes out to equal approximately the film thickness. b) Stacking faults and lattice distortions are not discernable by profile analysis of the diffraction peaks of the gold films investigated here.

4. Resistivity Measurements

A few of the silicon crystals were predeposited in a separate UHV apparatus at two ends with 2 μm thick molybdenum films for later electrical contact. Four

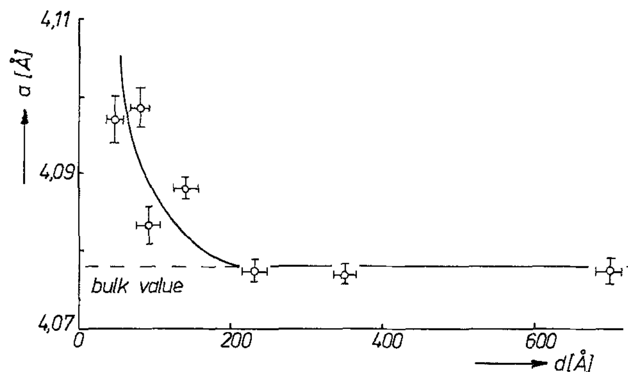

Fig. 12. Thickness dependence of lattice parameter a of evaporated gold films

normal pressure contacts as shown in Fig. 13 schematically are used for determining electrical resistivity with the help of a compensation method. The measuring head of the quartz thickness monitor was arranged directly near the sample in the same plane, further details of the experimental set-up are described elsewhere [30, 31].

As mentioned in Section 1, the $\sqrt{3}$-superstructure of the silicon surface is obtained by heating up the crystal after deposition of a 20 Å thick gold film. The high resistivity of silicon substrate remains practically unchanged after this procedure. The following evaporation at room temperature causes the resistivity to fall very rapidly in the region 0–8 Å. Above 8 Å the curve flattens out, which can be seen from Fig. 13. It is interesting to compare this curve with similar curves obtained for gold films deposited on mica [32] or glass [33]. Obviously the resistivity in the present case shows an extra-ordinarily low value. This point becomes specially clear, if the measured values (open circles in Fig. 13) are compared with those calculated from size

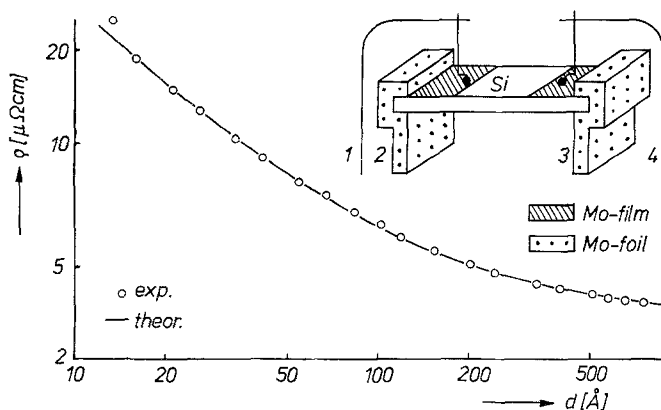

Fig. 13. Thickness dependence of the resistivity ϱ of evaporated gold films; [○] experimental points; [–] calculated according to (4)

effect theory of Fuchs and Sondheimer according to the relation [34]

$$\varrho = \varrho_0 \left[1 + \frac{3}{8}(1-p)\frac{l_0}{d}\right], \tag{4}$$

where ϱ_0 is the resistivity of the bulk with same density of lattice defects as the film, l_0 is the corresponding mean free path of the electrons, and p is the fraction of electrons specularly reflected at the film surfaces. The calculated curve is plotted in Fig. 13 as solid curve, demonstrating an astonishingly good agreement with almost all experimental points in the full thickness range. The typical rapid increase of resistivity values at about 200 Å due to coagulation effects [32] is absent completely in the present case. The values of the characteristic parameters of (4) are obtained as follows:

$\varrho_0 = 2.8\ \mu\Omega\text{cm}$ and $(1-p)\,l_0 = 260$ Å.

These values show only little deviations from the bulk gold values, namely [33]

$\varrho_0 = 2.2\ \mu\Omega\text{cm}$ and $l_0 = 380$ Å.

The slightly higher ϱ_0-value of the gold films indicates, that the films still possess a certain disorder in the volume. The comparison of l_0-values leads to $p = 0.3$. In agreement with other authors [33] it comes out, that the conduction electrons suffer largely diffused scattering at the film surfaces. That so small p-values are obtained inspite of the single-crystal structure of the film, might be due to silicon diffusion up to the film surface thus providing new scattering centers at the surface. Indeed, much higher p-values are obtained for silver films deposited under comparable conditions [35]. Through these silver films silicon diffusion cannot be detected at room temperature. That the silicon atoms are present on the gold surface and may be considered as scattering centers for the conduction electrons, is further demonstrated by a surprising result obtained for these films, namely: The resistivity *decreases* by about 1.5% for a 100 Å thick film after air inlet. For the case of a normal gold film this result is quite unexpected, because no gas adsorption takes place on pure gold surfaces at room temperature. A possible explanation for this can be the oxidation of the silicon present on the film surface, which should decrease the scattering cross section for the conduction electrons of the gold film.

5. Discussions and Conclusions

The results presented in the preceding sections give a relatively complete picture of the gold films investigated here. The films exhibit, in the whole region of thickness 10–1000 Å, a continuous shape without formation of holes and islands. They show a strongly marked (111)-orientation and only contain twinning faults to a certain extent. The film boundaries show an extraordinary plane parallel structure, which is reflected in the appearance of satellites at the side of the X-ray diffraction peaks, and in the extremely low resistivity values in the small thickness region. To the best of our knowledge no other system is known, to date, where both of these effects become so clear.

A further pecularity of these films is the presence of mosaic structure even for the thicker films and a marked increase of lattice constant for thicknesses below 100 Å. Additional distortions are caused by diffusion of silicon atoms to the gold film surface. Evidence for the presence of silicon at the film surface is provided by the splitting of silicon Auger peaks and by a decrease of resistivity after oxygen exposure. Nevertheless, these films behave in various respects as the bulk gold crystals. They can be used as an ideal model system specially where the homogenity of the films even for small thicknesses is important.

Acknowledgements. The authors wish to express their thanks to Prof. Dr. G. Wedler for his kind interest in the progress of this work. Financial help of "Deutsche Forschungsgemeinschaft" is thankfully acknowledged.

References

1. A.C.Tickle: *Thin Film Transistors* (John Wiley Sons, New York 1969) pp. 121
2. J.L.Lambert: Wiss. Ber. AEG-Telefunken **45**, 4 (1972)
3. G.Wedler: *Chemisorption* (Butterworths, London 1976)
4. A.Masson, R.Kern: J. Crystal Growth **2**, 227 (1968)
5. E.Bauer, H.Poppa: Thin Solid Films **12**, 167 (1972)
6. A.Hiraki, E.Lugujjo, J.W.Mayer: J. Appl. Phys. **43**, 3643 (1972)
7. A.K.Green, E.Bauer: J. Appl. Phys. **47**, 1284 (1976)
8. W.Fischer, P.Wissmann: Z. Naturforsch. **31**a, 183 (1976)
9. P.Wissmann: In G.Höhler (ed.); Springer Tracts Mod. Phys. **77**, 1 (1975)
10. C.C.Chang: Surface Sci. **23**, 283 (1970)
11. R.E.Schlier, H.E.Farnsworth: J. Chem. Phys. **30**, 917 (1959)
12. J.J.Lander, J.Morrison: J. Chem. Phys. **37**, 729 (1962)
13. H.F.Hadamovski (ed.): *Halbleiterwerkstoffe* (Deutscher Verlag für Grundstoffindustrie, Leipzig 1972)
14. W.Haidinger, S.C.Barnes: Surface Sci. **20**, 313 (1970)
15. P.Wissmann, Y.Summa: Vakuum-Technik **22**, 116 (1973)
16. M.P.Seah: Surface Sci. **32**, 703 (1972)
17. D.C.Jackson, T.E.Gallon, A.Chambers: Surface Sci. **36**, 381 (1973)
18. C.J.Powell: Surface Sci. **44**, 29 (1974)
19. K.Nakashima, M.Iwami, A.Hiraki: Thin Solid Films **25**, 423 (1975)

20. J.T.Grant, T.W.Haas: Surface Sci. **23**, 347 (1970)
21. K.Müller: In G.Höhler (ed.): Springer Tracts Mod. Phys. **77**, 97 (1975)
22. G.Wassermann, J.Grewen: *Texturen metallischer Werkstoffe* (Springer, Berlin 1962)
23. W.Fischer, P.Wissmann: Z. Naturforsch. **31**a, 190 (1976)
24. H.G. van Bueren: *Imperfections in Crystals* (North-Holland, Amsterdam 1961) pp. 322
25. H.Neff: *Grundlagen und Anwendungen der Röntgenfeinstrukturanalyse* (Verlag R.Oldenburg, München 1962)
26. R.W.Vook: In J.W.Anderson (ed.): *Epitaxial Growth*, Part A (Academic Press, New York 1975) pp. 339
27. W.Fischer, P.Wissmann: To be published
28. K.Sagel: *Tabellen zur Röntgenfeinstrukturanalyse* (Springer, Berlin-Heidelberg-New York 1958) p. 61
29. R.W.Vook, S.Ouyang, M.A.Otooni: Surface Sci. **29**, 277 (1972)
30. J.Feder, P.Rudolf, P.Wissmann: Thin Solid Films **36**, 183 (1976)
31. P.Rudolf, P.Wissmann: Vakuum-Technik **35**, 242 (1976)
32. K.L.Chopra, L.C.Bobb, M.H.Francombe: J. Appl. Phys. **34**, 1699 (1963)
33. H.G.Kadereit: Thin Solid Films **1**, 109 (1967)
34. K.L.Chopra: *Thin Film Phenomena* (McGraw-Hill Book Co., New York 1969)
35. P.Rudolf: Dissertation, University Erlangen-Nürnberg (1976)